Resolving the dynamic structure of chlorosomes in green sulfur bacteria by MAS NMR

Dsouza, L.A.

Chapter 5

Structure and dynamics of chlorosomes from the *bchR* mutant of *Chlorobaculum tepidum*

Abstract

In nature, one of the most remarkable light-harvesting structures is the chlorosome, a specialized organelle found in green photosynthetic bacteria, such as in Chlorobaculum tepidum. These chlorosomes contain densely packed molecules of bacteriochlorophyll (BChls), which are intricately arranged to maximize their ability to capture light energy. This unique configuration enables these bacteria to thrive in extreme environments where light is scarce. In this chapter, we focused on chlorosomes from the *bchR* mutant, which displays variation in the methylation patterns at 12^1 BChl side chain. To explore structural and dynamic changes, we utilized magic angle spinning nuclear magnetic resonance (MAS NMR). This sophisticated technique provides detailed insights into the atomic-level structure and dynamics of the chlorosome, illuminating how the bacteriochlorophylls are meticulously organized within this self-assembled supramolecular complex to enhance their function as light-harvesting antennas. We employed several experimental methods, including Cross-Polarization (CP), Direct-Polarization (DP), and Insensitive Nuclei Enhanced by Polarization Transfer (INEPT), as well as a DYSE strategy to effectively quantify both the rigid and flexible components of the system. Furthermore, we utilized two-dimensional ^{13}C experiments, such as RFDR and CHHC/CP3, to accurately assign signals and measure important distance constraints. Our findings revealed that the distance constraints obtained through CHHC analysis indicated the presence of a *syn-anti* alternating parallel stacking motifs within the *bchR* mutant chlorosomes. Initial observations of the dynamics, achieved through the DYSE approach, suggest contrasting dynamics between macrocycles and side chains, very similar to chlorosomes from the wild type (WT) or the mutant *bchQ*.

5.1 Introduction.

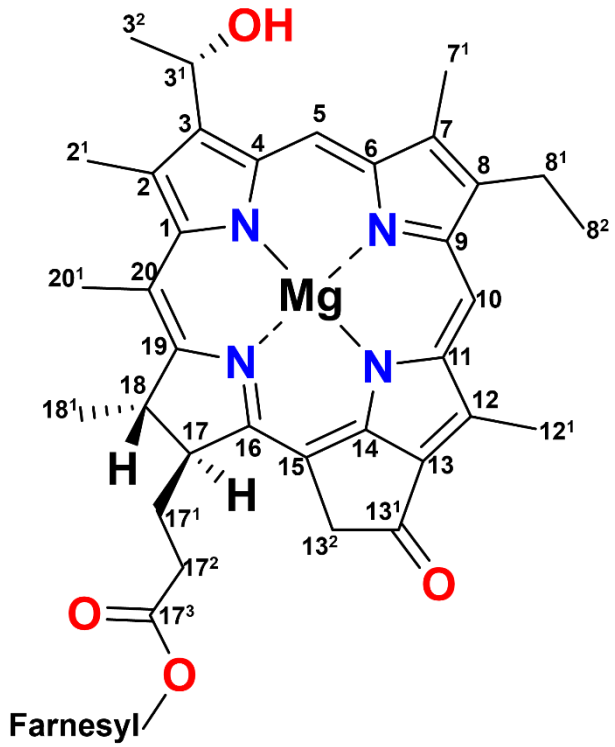

Figure 5.1 shows the chemical structure of [8Et, 12Me] BChl *c*, which is the most abundant BChl *c* homolog in chlorosomes of the *bchR* mutant.

The primary process in photosynthesis is harvesting sunlight and converting harvested light into useful chemical energy. This is achieved by chlorosomes in green bacteria that grow in anoxic and sulfur rich environments. The green sulfur bacterium *Chlorobaculum tepidum* is a model for the green bacteria and is known for the efficient conversion of harvested light even though it lives in sediments or dense microbial mats.[1–3] The harvested light is transferred to the FMO complex via the baseplate and to the reaction centre where charge separation takes place.[4] The chlorosome is an antennae organelle that is 100-200 nm in length, 50-60 nm in diameter, and contains bacteriochlorophyll *c* (BChl *c*) as the main pigment. The chlorosomes contain a self-aggregated pigment assembly without proteins involved in aggregation.[5–7] The BChls are organized basically with three main intermolecular interactions, coordination of Mg^{2+} with the 3^1-hydroxyl groups, hydrogen bonding between 13^1 carbonyl groups and 3^1 hydroxyl groups, and pi-pi stacking interactions between the chromophores.[8,9]The structure of the chlorosome differs with the growth conditions and its variability in size, composition, and heterogeneity of the packing makes it difficult to understand the structure. Different

techniques need to be combined to deduce the structure, and the combination of cryo-EM, solid-state NMR, optical spectroscopy and computer simulations has provided converging and convincing evidence that the BChl assemblies in chlorosomes can be described as a tubular plastic crystal composed of *syn-anti* parallel stacks forming sheets and concentric tubes.[9–12]

In this chapter, I briefly report on the *bchR* mutant of *Cba. tepidum*. The *bchR* mutant chlorosomes that are used in the present study differ from the WT in the methylations at only one position in the BChl side chains, since at the 12^1 position it contains only a methyl group (Figure 5.1). The presence of a single methylation at 12 gave rise to 3 homologs, [8Et, 12Me], [8Pr, 12Me], and [8Bu, 12Me].[13] This chemical heterogeneity was experimentally tested with HPLC using a previously reported protocol which is shown in Figure 5.2.[14]

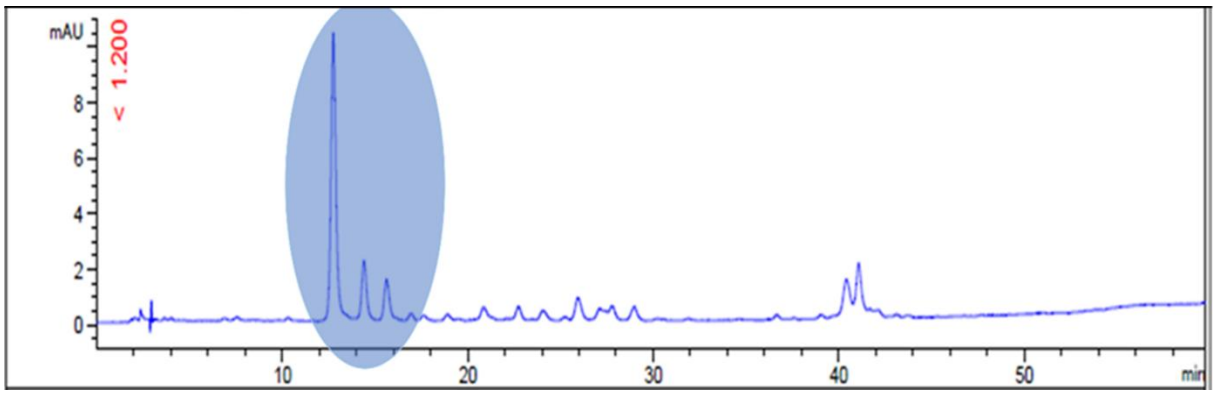

Figure 5.2 Chromatogram of *bchR*. The signal between 10-20 min retention time corresponds to BChls. The highest intensity signal in the highlighted region is the major homolog [8Et, 12Me] for the *bchR*.

The structure of the BChl *c* in chlorosomes from the *bchR* mutant was determined based on cryo-EM and Optical spectroscopy by Gunther *et al.*[11,15] In this work, we make use of solid-state NMR spectroscopy which gives atomic-level resolution to study the structure and dynamics of *bchR chlorosomes*. The Fourier transformation of the cryo-EM data for the *bchR* chlorosomes showed similar results as for WT with a spacing of 2.1 nm between tubes and a weak layer line at $1/1.24nm^{-1}$.[11] The similarity between WT and *bchR* suggests a similar structural model for the mutant. Since the *bchR* showed a decrease in full width at half maximum (fwhm) of the Q_y absorption band from $900cm^{-1}$ for WT to $540cm^{-1}$ for *bchR* mutant chlorosomes, this reflects a significant reduction of the structural heterogeneity.[11] MAS NMR can help to resolve the structure and dynamics of *bchR* chlorosomes in

comparison with the WT, and obtain a bottom-up view of the supramolecular packing of *bchR* mutant with its reduced heterogeneity.[9]
Similar to the work presented on *bchQ* chlorosomes in chapter 3, we employed one-dimensional CP, DP, INEPT, and two-dimensional RFDR to assign the signals and the obtained carbon chemical shifts were used to calculate the aggregation shifts. The spin diffusion-based CHHC/CP3 was performed to resolve distance constraints at 277K for a uniformly labelled sample and the results are compared with available data for the WT.

5.2 Materials and Methods.

5.2.1 Sample Preparation

The *Chlorobaculum tepidum* (*Cba. tepidum*) strain of the *bchR* mutant was grown anaerobically at 40 degrees in Wahlund medium[16] in 1.0 L culture bottles with continuous slow stirring and illumination with fluorescent tubes (Osram, mixture of 18W/25 universal white and 18W/77 Floura) using high light conditions to reduce sample heterogeneity. For uniform labeling with ^{13}C for MAS experiments, 1.0 L of the Wahlund medium was inoculated with 75 mL freshly grown culture without ammonium acetate in it and grown for two days for light adaptation and growth. Once it was grown, 75 mL of this culture was transferred to a medium that contained only ^{13}C enriched ammonium acetate as the sole carbon source.[7] Sample purification followed the procedures described in Tian *et al* for single chlorosomes.[17] For solid-state NMR studies, the sample was further concentrated at 200000×g for 1 hour using an ultracentrifuge, and the obtained pellet was used to fill the NMR rotor in the form of a paste.

5.2.2 Solid-State NMR Measurements

All solid-state NMR experiments were performed with a Bruker AV-750 spectrometer equipped with a 3.2 mm triple resonance MAS probe head (Bruker, Karlsruhe, Germany), using a ^{13}C radiofrequency of 188.6 MHz. Two different temperatures were used to study the effect of temperature on the structure and dynamics. Spinning frequencies of 20 kHz were used for all 1-D measurements and 11 kHz was used for 2-D measurements. Spinal 64 decoupling was used to decouple the proton magnetic moments during acquisition.[18] 2-D ^{13}C-

^{13}C dipolar correlation spectra were recorded using the radio frequency driven recoupling (RFDR) sequence with phase-sensitive detection in ω_1 with 1.4, 3.2,5.2, or 9.2 ms mixing times to probe short, medium, or long-range correlations.[19] For each of the 256 steps in the indirect dimension, 128 scans were collected. 2-D ^{13}C-^{13}C spectra were recorded using the CHHC sequence for indirect detection of ^{1}H-^{1}H contacts with ^{1}H spin diffusion times of 250 μs[20–22]. The initial CP contact time was set to 512 μs and short contact times of 128 μs were used to enclose the ^{1}H-^{1}H diffusion step to ensure polarization transfer to directly bonded ^{1}H-^{13}C pairs. For each of the 256 steps in the indirect dimension, 128 scans were collected. One dimensional measurement cross polarization (CP) and insensitive nuclei enhanced by polarization transfer (INEPT) measurements were performed with 1k scans. The delay was set to 2 s for CP and delay periods of 1.75 ms or 1.15 ms were used for INEPT. The proton π/2 pulse length for the CP was 2.5 μs at 100 kHz RF amplitude.

5.3 Results and Discussion

The ^{13}C chemical shift assignments corresponding to the chlorosomes of the *bchR* mutant were determined using a high-resolution two-dimensional homonuclear ^{13}C-^{13}C correlation spectroscopy dataset, as illustrated in Figure 5.3. In comparison with the RFDR spectra obtained for the wild type (WT), the mutant spectra display substantially enhanced resolution. This improvement signifies a greater degree of local molecular ordering within the packing arrangement of BChl *c* in the *bchR* mutant. Despite this increase in spectral clarity, the observed ^{13}C chemical shifts of the mutant remain largely consistent with those of the WT, indicating that the overall electronic environment of the chlorosomal pigments is only minimally altered. Furthermore, the characteristic ratio of principal doubling, approximately 7:3, between hydrogen-bond donor and non-donor groups at the C-5 and C-71 positions was also detected in the *bchR* mutant, suggesting that the fundamental hydrogen-bonding interactions within the pigment network are preserved.

A comprehensive summary of the ^{13}C chemical shift assignments is presented in Table 5.1. These values served as the basis for calculating the aggregation-induced chemical shift differences, which are depicted in Figure 5.3. Notably, the 2^1, 3, 3^2, 5, 12, 12^1, and 14 carbons positions exhibited deviations of $\geq|2.5|$ ppm relative to the corresponding chemical shifts of monomeric BChl *c* in solution.[7]

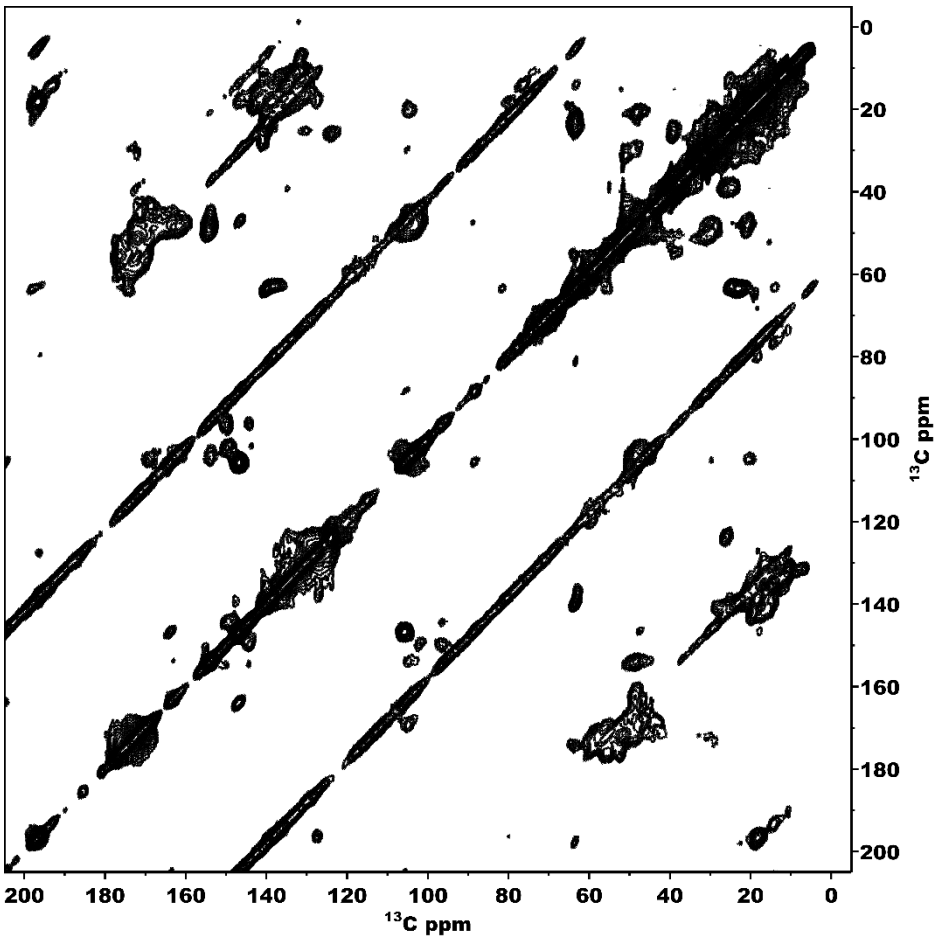

Figure 5.3 shows the RFDR spectrum collected at 277 K with 9.2 ms mixing time to probe the long-range couplings along with the short-range couplings.

Table 5.1 Chemical shifts of ^{13}C (ppm) in chlorosomes of the *Cba. tepidum bchR* mutant: liquid σ_{liq}^{C}, solid-state σ_{s}^{C} and aggregation shifts $\Delta\sigma_{s}^{C} = \sigma_{s}^{C} - \sigma_{liq}^{C}$

Position	σ_{liq}^{C} (Balaban *et al*. 1995)[7]	σ_{s}^{C} chlorosomes	$\Delta\sigma_{s}^{C}$ chlorosomes
1	153.76	153.67	-0.09
2	135.19	135.48	0.29
3	145.14	140.07	-5.07
4	145.28	144.45	-0.83
5	100.16	95.96	-4.2
6	150.69	150.09	-0.6
7	133.63	131.96	-1.67
8	143.48	143.18	-0.3
9	146.09	146.99	0.9

10	105.61	105.6	-0.01
11	147.66	147.07	-0.59
12	133.34	138.67	5.33
13	131.02	127.46	-3.56
14	161.08	163.96	2.88
15	104.92	103.97	-0.95
16	154.27	154.2	-0.07
17	50.14	50.87	0.73
18	48.19	48.79	0.6
19	167.84	169.79	1.95
20	104.68	104.5	-0.18
2^1	16.95	13.79	-3.16
3^1	65.14	63.81	-1.33
3^2	25.58	22.58	-3
7^1	10.55	10.74	0.19
8^1	19.24	18.68	-0.56
8^2	17.14	*	
12^1	12.29	18.07	5.78
13^1	198.2	196.74	-1.46
13^2	49.14	48.59	-0.55
17^1	29.69	29.54	-0.15
17^2	30.7	30.76	0.06
17^3	173.73	173.09	-0.64
18^1	20.55	20.63	0.08
20^1	21.14	20.39	-0.75
F1	61.3	59.99	-1.31
F2	117.51	118.84	1.33
F3	142.43	142.24	-0.19
F4	39.33	39.31	-0.02
F5	26.35	26.57	0.22
F6	123.28	123.99	0.71
F7	135.14	134.81	-0.33
F8	39.14	38.94	-0.2

F9	25.83	24.25	-1.58
F10	123.98	124.65	0.67
F11	131.02	130.9	-0.12
F12	25.24	25.27	0.03
$F3^1$	15.98	15.87	-0.11
$F7^1$	15.55	14.61	-0.94
$F11^1$	17.24	**	

* 8^2 signals could not be resolved from the 8^1 signals

** $F11^1$ signal could not be resolved.

Chemical shifts in brackets are another component in the system.

***The 2^1,3,3^2,5,12,12^1, and 14 carbons are shifted by 2.5 ppm or more with respect to solution state data.

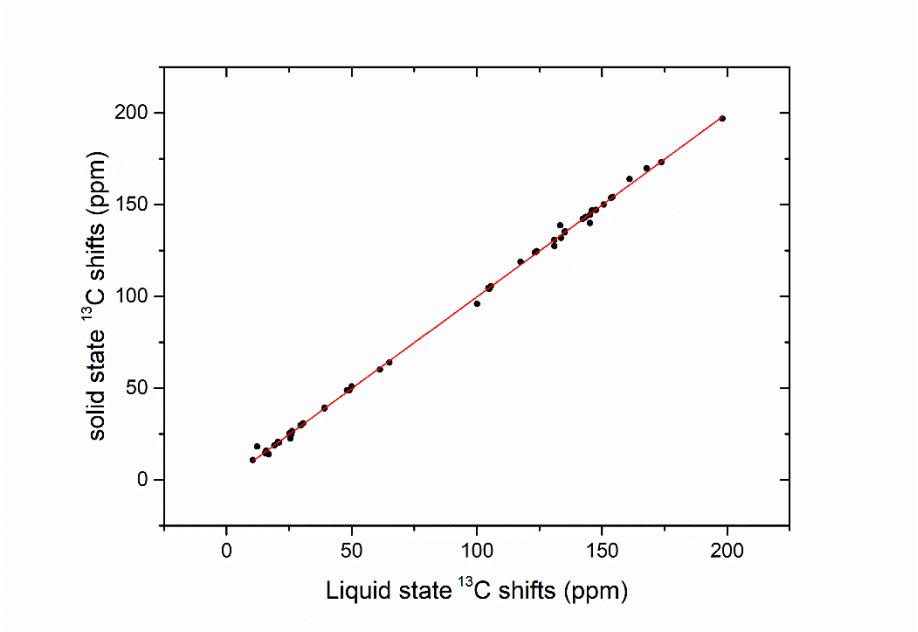

Figure 5.4 shows a chemical shift correlation plot for *bchR* mutant chlorosomes. The ^{13}C shifts in the solid-state NMR data are plotted against the monomer shifts from solution NMR data. The solid line represents the diagonal. The filled circles representing ^{13}C deviating from the solid line correspond to the aggregation shifts due to neighbouring BChl molecules.

To extend the analysis from resonance assignment to the derivation of distance constraints, proton-mediated correlation spectroscopy was employed using short mixing times of 350 μs. This approach enabled the extraction of internuclear distance constraints that are critical for

molecular-level structure determination. In particular, correlations between the C-13^2 and C-3^1 carbons were detected in the CHHC spectra, as highlighted in Figure 5.5, thereby providing direct evidence of spatial proximities within the aggregated BChl *c* assemblies.

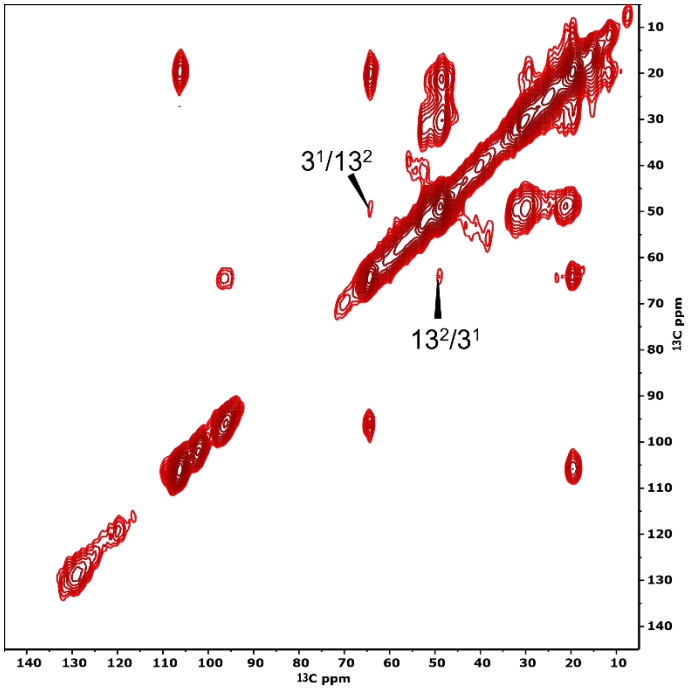

Figure 5.5 shows ^{13}C–^{13}C CHHC data for chlorosomes of the *bchR* mutant recorded at 277 K in a field of 17.6 T with 20 kHz spinning frequency. A ^1H–^1H spin diffusion mixing time of 350 μs was used. Intermolecular correlations are labeled in the spectrum.

The dynamic behaviour of the chlorosomes was examined through one-dimensional ^{13}C CP, DP, and INEPT experiments, with direct comparisons made to WT data (Figure 5.6). While DP detects signals from all molecular components, CP and INEPT function as dynamic filters, emphasizing rigid and flexible sites, respectively.[23] The spectral patterns observed for the *bchR* mutant closely resembled those of the *bchQ* mutant, suggesting common structural consequences of these mutations.

In the INEPT spectra (Figure 5.6a), resonances corresponding to dynamic segments for *bchR* (Pink) and WT (Green), such as F1-CH_2, F4-CH_2, F5-CH_2, F10-CH, F-3^1-CH_3, and side chains 17-CH, 18-CH, 17^1-CH_2, 17^2-CH_2, 32-C, 2^1-C, 7^1-C, 8^1-C, 8^2-CH_3 were detected. The *bchR* spectra displayed increased intensity in the 65–80 ppm range and near 100 ppm,

attributable to galactolipids.[7] A similar trend was previously reported for *bchQ* mutant chlorosomes.

The CP spectra (Figure 5.6b) highlighted rigid ^{13}C sites for *bchR* (Cyan) and WT (Red), including 13^1C, 17^3C, 14C, 16C, 1C, 6C, 9C, 4C, 3C, 2C, 10C, 15C, 5C, 3^1CH, $F1CH_2$, 17CH, 18CH, 17^1CH_2, 17^2CH_2, $F8CH_2$, $F5CH_2$, 3^2CH_3, $F3^1CH_3$, 2^1CH_2, $7^1(II)CH_3$. Overlaps between the 20-C and 5C(II) signals with the 10-C resonance were noted. Signals in the aliphatic region appeared broadened, consistent with homonuclear dipolar couplings characteristic of rigid molecular environments.

Finally, the DP spectra (Figure 5.6c) revealed all ^{13}C resonances regardless of mobility for *bchR* (Blue) and WT (Orange) , with *bchR* showing stronger signals relative to WT in the 60-80 ppm and 100 ppm regions. These signals originate from the sugar headgroups of galactolipids and the anomeric carbons of the surrounding environment. The enhanced lipid contribution relative to BChl in *bchR* chlorosomes points to an increased lipid-to-pigment ratio. This observation is consistent with transmission electron microscopy (TEM) findings showing reduced chlorosome size in the *bchR* and *bchQ* mutants compared with WT, suggesting a shared structural adaptation driven by these genetic modifications.[13]

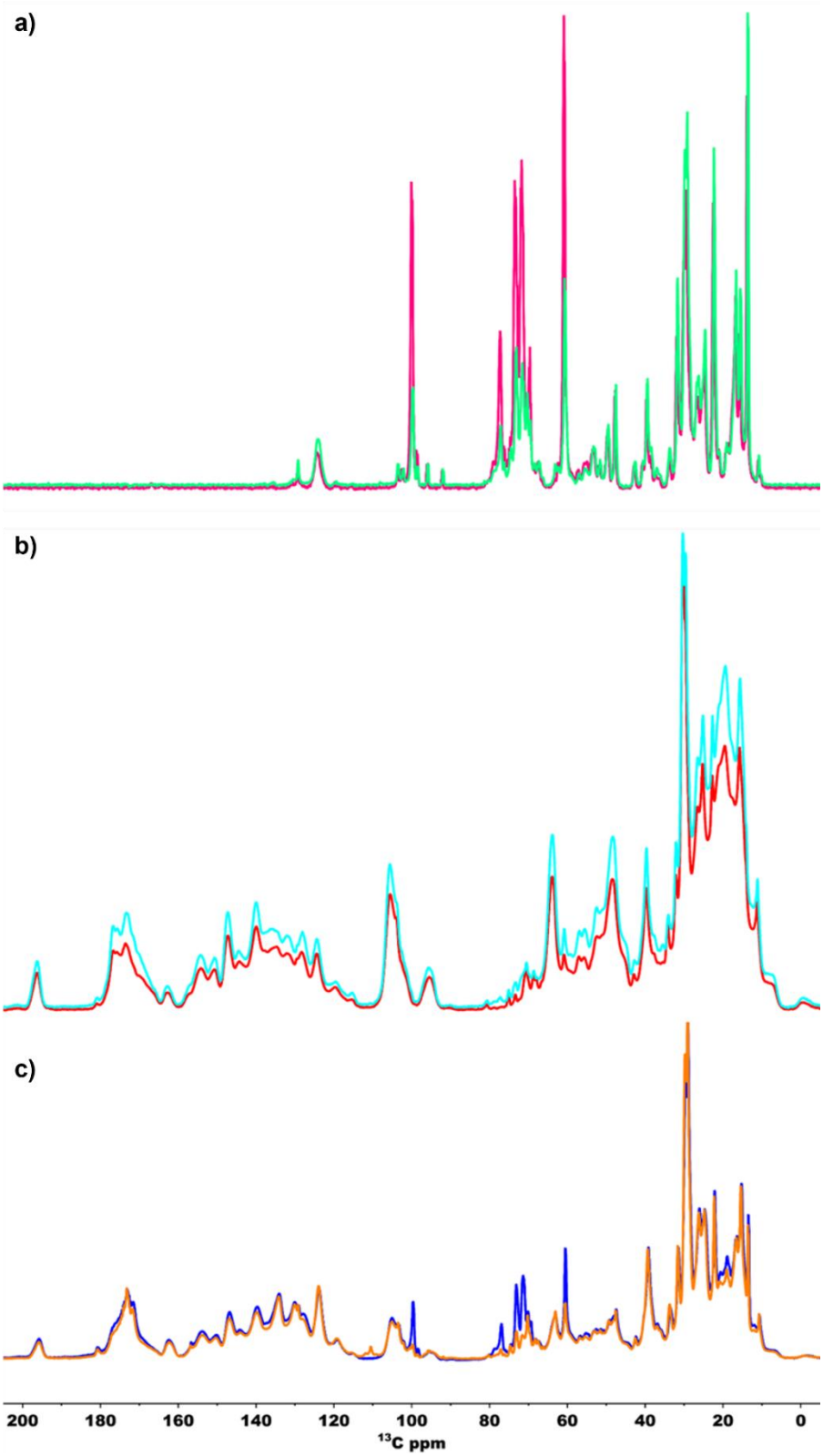

Figure 5.6 a) b) and c) represent Overlaid INEPT, CP, and DP spectra of *bchR* (Pink, Cyan, Blue) and WT (Green, Red, Orange), respectively, recorded in a 3.2 mm rotor spinning at 20 kHz at 277 K. The DP, CP, and INEPT spectra were normalised at the highest intensity.

5.4 Conclusion and Outlook

The variation in methylation at the C-12[1] side chain of BChl in *bchR* mutant chlorosomes displayed patterns consistent with those observed in the *bchQ* mutant and the wild type (WT). To unravel these similarities, we applied magic-angle spinning nuclear magnetic resonance (MAS NMR), which provides high-resolution insights into the atomic-level structure and dynamics of pigment–protein assemblies. Using RFDR datasets, we achieved resonance assignments, while CHHC/CP3 experiments supplied crucial distance constraints, revealing alternating *syn-anti* parallel stacking in the *bchR* mutant. Additional characterization with the DYSE method highlighted distinct differences in the motions of macrocyclic backbones versus side chains, a dynamic profile that mirrors the behaviour of WT and *bchQ* chlorosomes. Together, these findings shed light on the intricate interplay between pigment arrangement, side-chain modifications, and dynamic flexibility in bacterial light-harvesting systems.

References

(1) Overmann, J.; Cypionka, H.; Pfennig, N. An Extremely Low-Light Adapted Phototrophic Sulfur Bacterium from the Black Sea. *Limnology and Oceanography* **1992**, *37* (1), 150–155. https://doi.org/10.4319/lo.1992.37.1.0150.

(2) Beatty, J. T.; Overmann, J.; Lince, M. T.; Manske, A. K.; Lang, A. S.; Blankenship, R. E.; Van Dover, C. L.; Martinson, T. A.; Plumley, F. G. An Obligately Photosynthetic Bacterial Anaerobe from a Deep-Sea Hydrothermal Vent. *Proceedings of the National Academy of Sciences* **2005**, *102* (26), 9306–9310. https://doi.org/10.1073/pnas.0503674102.

(3) Prokhorenko, V. I.; Holzwarth, A. R.; Müller, M. G.; Schaffner, K.; Miyatake, T.; Tamiaki, H. Energy Transfer in Supramolecular Artificial Antennae Units of Synthetic Zinc Chlorins and Co-Aggregated Energy Traps. A Time-Resolved Fluorescence Study ᵗ. *J. Phys. Chem. B* **2002**, *106* (22), 5761–5768. https://doi.org/10.1021/jp0125754.

(4) Holzwarth, A. R.; Griebenow, K.; Schaffner, K. Chlorosomes, Photosynthetic Antennae with Novel Self-Organized Pigment Structures. *Journal of Photochemistry and Photobiology A: Chemistry* **1992**, *65* (1), 61–71. https://doi.org/10.1016/1010-6030(92)85032-P.

(5) Orf, G. S.; Blankenship, R. E. Chlorosome Antenna Complexes from Green Photosynthetic Bacteria. *Photosynth Res* **2013**, *116* (2–3), 315–331. https://doi.org/10.1007/s11120-013-9869-3.

(6) Oostergetel, G. T.; van Amerongen, H.; Boekema, E. J. The Chlorosome: A Prototype for Efficient Light Harvesting in Photosynthesis. *Photosynth Res* **2010**, *104* (2–3), 245–255. https://doi.org/10.1007/s11120-010-9533-0.

(7) Balaban, T. S.; Holzwarth, A. R.; Schaffner, K.; Boender, G.-J.; de Groot, H. J. M. CP-MAS 13C-NMR Dipolar Correlation Spectroscopy of 13C-Enriched Chlorosomes and Isolated Bacteriochlorophyll c Aggregates of Chlorobium Tepidum: The Self-Organization of Pigments Is the Main Structural Feature of Chlorosomes. *Biochemistry* **1995**, *34* (46), 15259–15266. https://doi.org/10.1021/bi00046a034.

(8) van Rossum, B.-J.; Steensgaard, D. B.; Mulder, F. M.; Boender, G. J.; Schaffner, K.; Holzwarth, A. R.; de Groot, H. J. M. A Refined Model of the Chlorosomal Antennae of the Green Bacterium *Chlorobium Tepidum* from Proton Chemical Shift Constraints Obtained with High-Field 2-D and 3-D MAS NMR Dipolar Correlation Spectroscopy. *Biochemistry* **2001**, *40* (6), 1587–1595. https://doi.org/10.1021/bi0017529.

(9) Ganapathy, S.; Oostergetel, G. T.; Wawrzyniak, P. K.; Reus, M.; Gomez Maqueo Chew, A.; Buda, F.; Boekema, E. J.; Bryant, D. A.; Holzwarth, A. R.; de Groot, H. J. M. Alternating Syn-Anti Bacteriochlorophylls Form Concentric Helical Nanotubes in Chlorosomes. *Proceedings of the National Academy of Sciences* **2009**, *106* (21), 8525–8530. https://doi.org/10.1073/pnas.0903534106.

(10) Ganapathy, S.; Oostergetel, G. T.; Reus, M.; Tsukatani, Y.; Gomez Maqueo Chew, A.; Buda, F.; Bryant, D. A.; Holzwarth, A. R.; de Groot, H. J. M. Structural Variability in Wild-Type and *BchQ BchR* Mutant Chlorosomes of the Green Sulfur Bacterium *Chlorobaculum Tepidum*. *Biochemistry* **2012**, *51* (22), 4488–4498. https://doi.org/10.1021/bi201817x.

(11) Günther, L. M.; Jendrny, M.; Bloemsma, E. A.; Tank, M.; Oostergetel, G. T.; Bryant, D. A.; Knoester, J.; Köhler, J. Structure of Light-Harvesting Aggregates in Individual Chlorosomes. *J. Phys. Chem. B* **2016**, *120* (24), 5367–5376. https://doi.org/10.1021/acs.jpcb.6b03718.

(12) *The role of chirality and plastic crystallinity in the optical and mechanical properties of chlorosomes | elsevier enhanced reader*. https://doi.org/10.1016/j.isci.2021.103618.

(13) Chew, A. G. M.; Frigaard, N.-U.; Bryant, D. A. Bacteriochlorophyllide *c* C-8 ^{2} and C-12 ^{1} Methyltransferases Are Essential for Adaptation to Low Light in *Chlorobaculum Tepidum*. *J Bacteriol* **2007**, *189* (17), 6176–6184. https://doi.org/10.1128/JB.00519-07.

(14) Frigaard, N.-U.; Takaichi, S.; Hirota, M.; Shimada, K.; Matsuura, K. Quinones in Chlorosomes of Green Sulfur Bacteria and Their Role in the Redox-Dependent Fluorescence Studied in Chlorosome-like Bacteriochlorophyll c Aggregates. *Arch Microbiol* **1997**, *167* (6), 343–349. https://doi.org/10.1007/s002030050453.

(15) Günther, L. M.; Löhner, A.; Reiher, C.; Kunsel, T.; Jansen, T. L. C.; Tank, M.; Bryant, D. A.; Knoester, J.; Köhler, J. Structural Variations in Chlorosomes from Wild-Type and a *BchQR* Mutant of *Chlorobaculum Tepidum* Revealed by Single-Molecule Spectroscopy. *J. Phys. Chem. B* **2018**, *122* (26), 6712–6723. https://doi.org/10.1021/acs.jpcb.8b02875.

(16) Wahlund, T. M.; Woese, C. R.; Castenholz, R. W.; Madigan, M. T. A Thermophilic Green Sulfur Bacterium from New Zealand Hot Springs, Chlorobium Tepidum Sp. Nov. *Arch. Microbiol.* **1991**, *156* (2), 81–90. https://doi.org/10.1007/BF00290978.

(17) Tian, Y.; Camacho, R.; Thomsson, D.; Reus, M.; Holzwarth, A. R.; Scheblykin, I. G. Organization of Bacteriochlorophylls in Individual Chlorosomes from Chlorobaculum Tepidum Studied by 2-Dimensional Polarization Fluorescence Microscopy. *J. Am. Chem. Soc.* **2011**, *133* (43), 17192–17199. https://doi.org/10.1021/ja2019959.

(18) Bräuniger, T.; Wormald, P.; Hodgkinson, P. Improved Proton Decoupling in NMR Spectroscopy of Crystalline Solids Using the S PINAL -64 Sequence. *Monatshefte f?r Chemie / Chemical Monthly* **2002**, *133* (12), 1549–1554. https://doi.org/10.1007/s00706-002-0501-z.

(19) Bennett, A. E.; Griffin, R. G.; Ok, J. H.; Vega, S. Chemical Shift Correlation Spectroscopy in Rotating Solids: Radio Frequency-driven Dipolar Recoupling and Longitudinal Exchange. *The Journal of Chemical Physics* **1992**, *96* (11), 8624–8627. https://doi.org/10.1063/1.462267.

(20) Lange, A.; Seidel, K.; Verdier, L.; Luca, S.; Baldus, M. Analysis of Proton−Proton Transfer Dynamics in Rotating Solids and Their Use for 3D Structure Determination. *J. Am. Chem. Soc.* **2003**, *125* (41), 12640–12648. https://doi.org/10.1021/ja034555g.

(21) Lange, A.; Becker, S.; Seidel, K.; Giller, K.; Pongs, O.; Baldus, M. A Concept for Rapid Protein-Structure Determination by Solid-State NMR Spectroscopy. *Angewandte Chemie International Edition* **2005**, *44* (14), 2089–2092. https://doi.org/10.1002/anie.200462516.

(22) *2D13C–13C MAS NMR Correlation Spectroscopy with Mixing by True 1H Spin Diffusion Reveals Long-Range Intermolecular Distance Restraints in Ultra High Magnetic Field | Elsevier Enhanced Reader*. https://doi.org/10.1006/jmre.2002.2588.

(23) Matlahov, I.; van der Wel, P. C. A. Hidden Motions and Motion-Induced Invisibility: Dynamics-Based Spectral Editing in Solid-State NMR. *Methods* **2018**, *148*, 123–135. https://doi.org/10.1016/j.ymeth.2018.04.015.